where $\delta = 0$ for clamped edges and $\delta = 1$ for simply supported edges. Substituting Eqs. (A2, A3, and A4) into Eq. (A1), it is readily verified that for $s \neq m$

$$\int_0^a \left\{ J_n\left(\alpha_{mn}\frac{r}{a}\right) - \frac{J_n(\alpha_{mn})}{I_n(\gamma_{mn})} I_n\left(\gamma_{mn}\frac{r}{a}\right)\right\}\left\{ J_n\left(\alpha_{sn}\frac{r}{a}\right) - \frac{J_n(\alpha_{sn})}{I_n(\gamma_{sn})} I_n\left(\gamma_{sn}\frac{r}{a}\right)\right\} rdr = 0 \quad \text{(A5)}$$

for both clamped and simply supported outer edges at $r = a$.

References

[1] Hirschberg, M. H. and Mendleson, A., "Analysis of Stresses and Deflections in a Disk Subjected to Gyroscopic Forces," TN-4218, 1958, NACA.

[2] Meirovitch, L., "Bending Vibrations of a Disk Subjected to Gyroscopic Forces," *Journal of the Astronautical Sciences*, Vol. 8, 1961, pp. 88–93.

[3] Johnson, M. W., "On the Dynamics of Shallow Elastic Members," *Proceedings of the Symposium on the Theory of Thin Elastic Shells (Delft)*, North-Holland, Amsterdam, 1960, pp. 281–300.

[4] Schlack, A. L. and Kessel, P. G., "Gyroscopically Induced Vibrations of Plates and Membranes," *AIAA Journal*, Vol. 6, No. 12, Dec. 1968, pp. 2360–2363.

[5] Timoshenko, S. and Woinowsky-Kreiger, S., *Theory of Plates and Shells*, McGraw-Hill, New York, 1959.

[6] Wah, T., "Vibration of Circular Plates," *Journal of the Acoustical Society of America*, Vol. 34, No. 3, 1962, pp. 275–281.

[7] Weiner, R. S., "Forced Axisymmetric Motions of Circular Elastic Plates," *Journal of Applied Mechanics*, Vol. 4, 1965, pp. 893–898.

[8] Stoker, J. J., *Nonlinear Vibrations*, Interscience, New York, 1950, Chap. VI.

[9] McLachlan, N. W., *Theory and Applications of Mathieu Functions*, Dover, New York, 1964.

OCTOBER 1969 AIAA JOURNAL VOL. 7, NO. 10

A Penetration Criterion for Double-Walled Structures Subject to Meteoroid Impact

J. P. D. WILKINSON*

General Electric Company, Schenectady, N.Y.

A penetration criterion is developed for double-walled structures subject to hypervelocity impact. During the impact, both the incoming particle and a portion of the front sheet are fragmented, and the resulting spray loads the rear sheet impulsively. The rear sheet is said to have failed when the strain it experiences exceeds the strain-to-fracture of the material. In this study the rear sheet response is followed into the elasto-plastic regime by means of an existing computer code. Based on the new criterion, it is shown how a rational choice of material properties may be made for the front and rear sheets of the structure. Finally, the penetration criterion is applied to the problem of calculating the optimum protection requirements for given spacecraft applications during interplanetary flight. Here, a Monte Carlo method is used to account for the observed distribution of meteoroid properties.

Nomenclature

A = exposed area
a,b = flux constants
c_1,c_2 = speed of sound in front and rear sheets
d = particle diameter
E = Young's modulus
m = particle mass
m_1 = mass per unit area of front sheet
m_2 = mass per unit area of rear sheet
m_* = mass of plug removed from front sheet
N = cumulative number of meteoroids
P_n = probability of n events or fewer
r = radial distance from impact point
S = spacing between front and rear sheets
T = time of exposure
t_1,t_2 = thickness of front and rear sheets
V = particle velocity
$\bar{V}_A$ = average axial spray velocity
$\bar{V}_R$ = average radial spray velocity
Δ = standard deviation of spray mass distribution
ϵ = strain, or ductility, or elongation
ϵ_{max} = maximum strain experienced by rear sheet
$\bar{\theta}$ = average cone angle of spray
ν = Poisson's ratio
ρ = particle density
ρ_1,ρ_2 = densities of front and rear sheets
σ = initial biaxial stress state due to pressurization
σ_u = ultimate stress
σ_y = yield stress
σ_{yt} = yield stress at 0.2% offset

Presented as Paper 68-1058 at the AIAA 5th Annual Meeting and Technical Display, Philadelphia, Pa., October 21–24, 1968; submitted September 27, 1968; revision received April 14, 1969. The author wishes to thank J. A. Mirabal and S. R. Woodall for their constructive suggestions and criticisms during the course of this investigation.

* Mechanical Engineer, Research and Development Center. Member AIAA.

Introduction

DURING a long interplanetary mission, there is, according to the best data available, a distinct possibility that a spacecraft will encounter meteoroids of such a size that considerable damage could be caused if adequate protection is not given to the spacecraft, its electronic components, and its fuel tanks. One way of doing this is to erect a thin shield a certain distance from the main structure. The shield then serves to fragment and perhaps vaporize an incoming hypervelocity particle, and the resulting debris spreads out in the form of a cone. The damage to the rear wall is thus considerably less than if the wall were unshielded.

The calculation of the penetration mechanics of a hypervelocity particle into such a structure is extremely complex. Several numerical methods based essentially on the hydro-

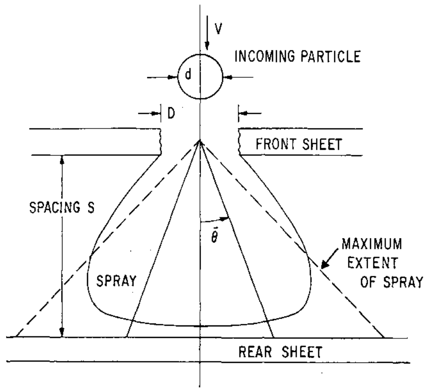

Fig. 1 Schematic of spray configuration.

dynamic flow of the particle and the structure are in existence, and can, in fact, be used to make penetration predictions. However, these hydrodynamic codes are so complex that their use is not economical in iterative design calculations. For such design calculations it is imperative to have a simple penetration criterion to predict whether or not the structure will be punctured by a given particle. It is the purpose of this paper to present such a penetration criterion for the impact of a meteoroid into a double-walled structure. The criterion is developed (as described below) by a combination of theory and of empirical correlations with existing experimental observations and numerical results from the aforementioned hydrodynamic codes. Two basic assumptions are made in the analysis. The first is that the front sheet completely fragments or vaporizes the incoming particle, and that no large solid fragments remain. The second is that the failure of the rear plate occurs as a bulge and a final tearing, or petalling, of the material.

Spray Dynamics

When a meteoroid particle penetrates the front sheet of a double-walled system it removes a certain amount of material from the sheet. The shock waves set up during the impact serve to fragment both the particle and the mass m_* so removed, and the combined mass flies toward the rear sheet in the form of a spray (see Fig. 1). The calculation of the spray dynamics will be made here by a modification of a simple mechanistic approach due to Madden.[1]

The average axial velocity $\bar{V}_A$ of the spray is determined by the condition that momentum is conserved during the impact. Thus,

$$\bar{V}_A = mV/(m + m_*) \tag{1}$$

The average radial velocity $\bar{V}_R$ is related to the average axial velocity $\bar{V}_A$ through the expression

$$\tan\bar{\theta} = \bar{V}_R/\bar{V}_A \tag{2}$$

where $\bar{\theta}$ is the average cone angle of the spray particle. In Madden's theory, the average cone angle appears to be larger than that observed experimentally. In addition, his theory does not predict a cutoff for the angle as observed. Thus, in the present development, we shall develop an empirical expression for $\tan\bar{\theta}$.

It has been observed experimentally that the spray expands in the form of a cone whose semivertex angle is always less than about 45°.[2,3] This phenomenon has also been observed in the results of the theoretical hydrodynamic computer codes such as VISTA[4] and CAMEO.[2] The average cone angle $\bar{\theta}$ is therefore certainly less than 45°. In the Appendix, an empirical expression for the average cone angle $\bar{\theta}$ is derived from the results of the aforementioned computer codes. The resulting expression is

$$\tan\bar{\theta} = \begin{cases} 0.6(m_1/\rho d)^{1/2}; & m_1/\rho d < 1 \\ 0.6 \quad ; & m_1/\rho d > 1 \end{cases} \tag{3}$$

The remaining development of the spray dynamics now follows Madden's theory. Experimental and theoretical observations indicate that the mass distribution m_d of the spray as it strikes the rear wall is approximately Gaussian. Thus, following Madden,[1] it is assumed that

$$m_d(r) = a \exp[-r^2/2\Delta^2] \tag{4}$$

where Δ is the standard deviation of the distribution. It may then be shown, as in Ref. 1, that

$$\Delta = (2/\pi)^{1/2}S\tan\bar{\theta},\ a = (m + m_*)/(4S^2\tan^2\bar{\theta}) \tag{5}$$

When the spray strikes the rear sheet, it imparts to it an impulsive velocity V_2. Because the total impulse experienced by the sheet occurs over a very short time, it is reasonable to require that momentum be conserved during the impact. It can then be shown that the initial velocity of the rear sheet is

$$V_2(r) = \frac{(1 + m_*/m)^{-1}V}{1 + 4S^2\tan^2\bar{\theta}(1 + m_*/m)^{-1}(m_2/m)\exp(r^2/2\Delta^2)} \tag{6}$$

If the condition

$$4m_2S^2\tan^2\bar{\theta} \gg m + m_* \tag{7}$$

holds, we obtain the initial velocity in the form

$$V_2(r) = \xi\exp(-r^2/2\Delta^2) \tag{8}$$

where

$$\xi = mV/(4m_2S^2\tan^2\bar{\theta}) \tag{9}$$

The condition (7) means physically that the mass of a circular portion of the rear sheet of radius $2S\tan\bar{\theta}$ is much greater than the combined mass of the particle and the mass m_* of the plug removed from the front sheet. It is found experimentally that the diameter of the plug may be up to 10 times the particle diameter, depending on the materials and impact velocities concerned.[2] Even in this case, the condition (7) is satisfied for most realistic spacings so that Eq. (8) represents a satisfactory expression for the initial velocity of the rear sheet.

Penetration Criterion

To develop a realistic penetration criterion, the response of the rear sheet to the applied initial velocity must be followed

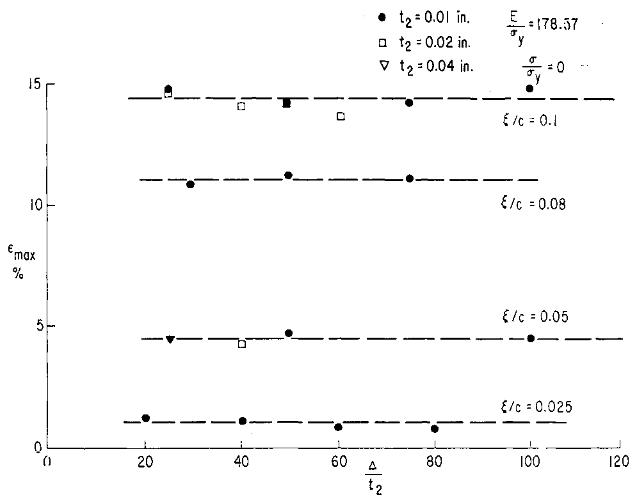

Fig. 2 Maximum strain experienced by rear sheet.

into the regions of large elastic and plastic deformations. In the development that follows, it will be assumed that the initial impulse is not severe enough to cause a spallation failure in the rear sheet. Rather, the sheet will be assumed to fail by bulging in a tensile manner, a failure mode that has been observed experimentally many times.[2] Because of the complexity of the equations of motion that govern the large-deflection response of plates to impulsive loadings, a numerical method of calculation must be employed. In this study, the computer code developed by Witmer, Balmer, Leech, and Pian[5,6] has been used. Even after recourse to a numerical method, the simulation of the precise details of the stress-strain relations for many materials is not feasible. Thus, in the calculations that follow, we have assumed that the rear sheet material is of the perfectly elastic, plastic type. The effects of strain hardening have therefore been ignored, as have those of the rate of strain. Because the impact area is fairly localized, it is assumed that the rear sheet can be replaced by a plate of infinite extent.

A suitable fracture criterion is the requirement that the maximum strain ϵ_{max} experienced by the sheet will exceed the strain-to-failure of the material (taken to be the elongation of a 2-in. gage length). The maximum strain may be expressed as

$$\epsilon_{max} = f[\xi,\Delta,E,\sigma_y,t_2,\rho_2,\sigma,\nu] \tag{10}$$

A dimensional analysis shows that

$$\epsilon_{max} = f[\xi/c_2,E/\sigma_y,\sigma/\sigma_y,\Delta/t_2,\nu] \tag{11}$$

Because ν is nearly the same for most common shielding materials, its value has been taken as $\frac{1}{3}$ for all subsequent work. Thus,

$$\epsilon_{max} = f[\xi/c_2,E/\sigma_y,\sigma/\sigma_y,\Delta/t_2] \tag{12}$$

By making a parametric numerical study using the computer code of Witmer et al., the functional relationship given in Eq. (12) can be precisely determined.

It was found during the numerical study that a finite clamped plate with a radius of 17 in. suitably represented the infinite plate in that the stresses at the boundary were always at least 2 orders of magnitude less than those near the center. In order to assess the effect of numerical roundoff due to the finite-difference scheme, various plate thicknesses were used. It was found that when the number of station points on the plate radius was 170, then the code tended to give inaccurate results for very concentrated loads ($\Delta/t_2 < 20$). For most realistic applications, however, $\Delta/t_2 > 20$, so that these inaccuracies have negligible effect on the final results. In Fig. 2 we show the results of the parametric study for a plate with the parameters $E/\sigma_y = 178.57$ and

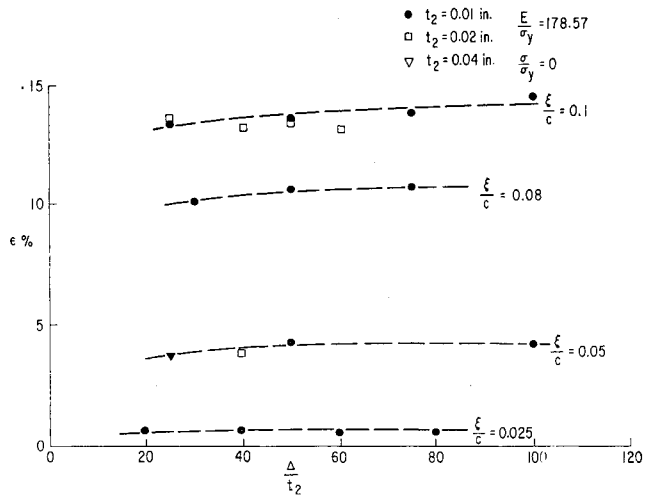

Fig. 3 Extensional strain component.

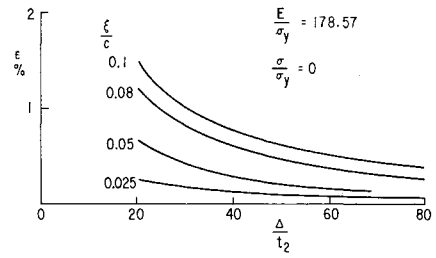

Fig. 4 Bending strain component.

$\sigma/\sigma_y = 0$. It will be observed that the maximum strain is virtually independent of the quantity Δ/t_2. This circumstance is important in that it simplifies Eq. (12) to the form

$$\epsilon_{max} = f[\xi/c_2,E/\sigma_y,\sigma/\sigma_y] \tag{13}$$

Figures 3 and 4 show the extensional and bending components of the maximum strain of Fig. 2. The extensional strain is by far the most dominant. It increases to an asymptotic value with increasing Δ/t_2. On the other hand, the bending strain decreases to zero as Δ/t_2 increases. A small value of Δ/t_2 represents the application of a relatively concentrated load, when bending strains may be expected to be large. The parametric study was continued using a constant value of $\Delta/t_2 = 40$. The final results are illustrated in Fig. 5. Here, the maximum strain ϵ_{max} is plotted as a function of ξ/c_2 and E/σ_y for the case of an initially unstressed plate ($\sigma/\sigma_y = 0$). The figure represents graphically the desired penetration criterion. For if a material fractures under an elongation of 20%, for example, and if it has a value of $E/\sigma_y = 260$, then any rear sheet made of that material will be penetrated by a given particle if ξ/c_2 exceeds 0.154. This allowable value of ξ/c_2 will be henceforth denoted by $(\xi/c_2)_a$.

In more detail, the penetration criterion may be stated as follows. Penetration will occur when

$$mV/4m_2S^2\tan^2\bar{\theta} \geq c_2(\xi/c_2)_a \tag{14}$$

Substituting the expression for $\tan\bar{\theta}$ from Eq. (2), it is seen that penetration occurs

1) when $m_1/\rho d > 1$,

$$1.44c_2(\xi/c_2)_a m_2S^2 \leq mV \tag{15}$$

2) when $m_1/\rho d < 1$,

$$1.44c_2(\xi/c_2)_a m_1m_2S^2 \leq m\rho dV \tag{16}$$

It can be shown that when $m_1/\rho d < 1$ (i.e., when the particle

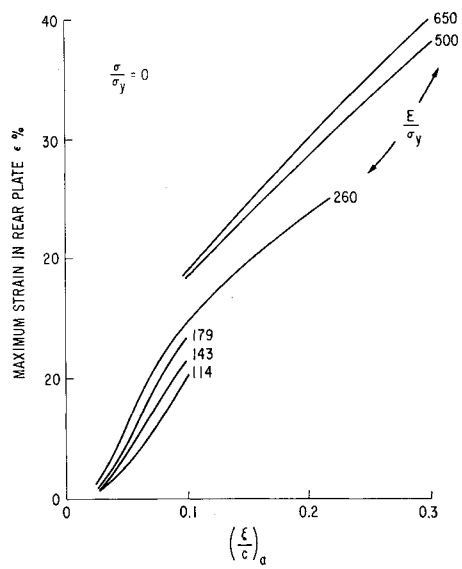

Fig. 5 Determination of maximum allowable ξ/c.

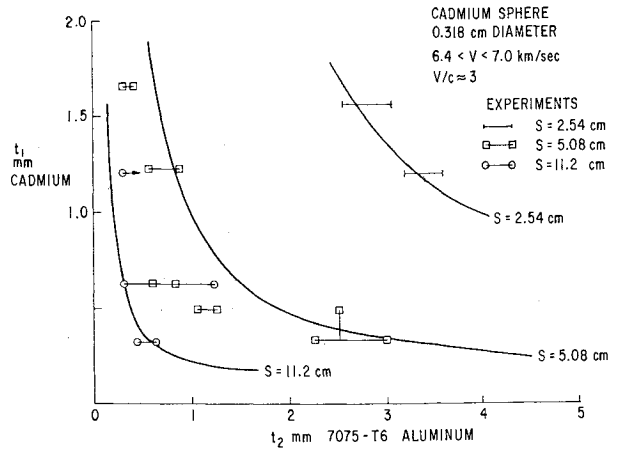

Fig. 6 Comparison of theory and experiments—cadmium.

is large compared with the plate thickness), then the optimum protection is obtained if $m_1 = m_2$, that is, if the masses per unit area of the front and rear sheets are equal. On the other hand, when $m_1/\rho d > 1$ (i.e., when the particle is small compared with the plate thickness), then the optimum protection is obtained when

$$m_1 = \rho d, \quad m_2 = \frac{mV}{1.44S^2 c_2(\xi/c_2)_a} \tag{17}$$

In this case the rear sheet thickness is proportional to the particle momentum, whereas the front sheet thickness is just sufficient to cause the spray to attain its maximum angular spread.

The effects of pressurization or prestress are felt through the parameter σ/σ_y. It was found during the numerical study that pressurization tended to increase the maximum strain only by as much as the initial strain due to pressurization σ/E. That is,

$$\epsilon_{\max}(p) \approx \epsilon_{\max}(u) + \sigma/E \tag{18}$$

where the subscripts p and u denote the pressurized and unpressurized states, respectively. Thus, for rear sheets of a ductile material the effect of pressurization will not be great, whereas for a brittle material it can be appreciable. This point will be discussed in more detail subsequently.

Comparisons of the predictions of the penetration criterion with the experimental results of McMillan[2] are shown in Figs. 6 and 7. Figure 6 shows the thickness of a cadmium front sheet and a 7075-T6 aluminum rear sheet that is required to just stop a spherical cadmium particle of diameter 0.318 cm and velocity between 6.4 and 7 km/sec. Figure 7 shows similar thickness requirements when the particle is a lead sphere. Both cases show excellent agreement with experiments. The agreement between experiment and theory in the case of an aluminum front sheet and an aluminum particle was not nearly so satisfactory. The theory underpredicted the thickness of the front sheet for a given rear sheet by about 60%. This may be attributed to the fact that the particle velocity in that case was only 1.5 times the speed of sound in the front sheet, so that complete fragmentation of the particle may not have occurred. In such cases it may be desirable (but conservative) to use a single sheet penetration criterion and to neglect the effect of the spacing between the sheets.

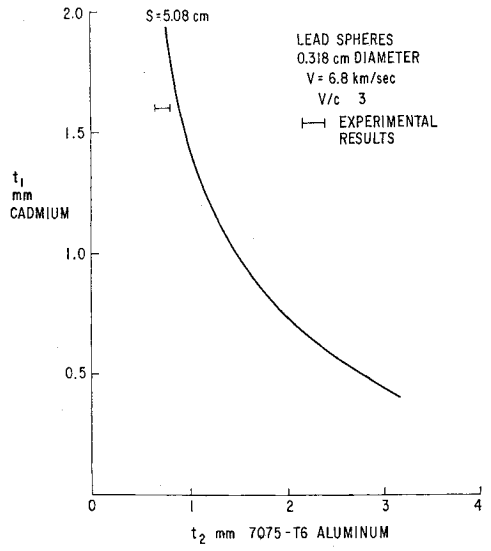

Fig. 7 Comparison of theory and experiments—lead.

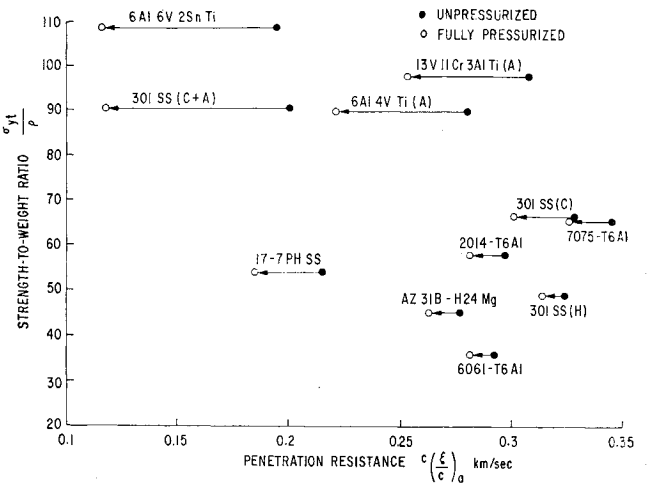

Fig. 8 Material selection for tankage walls.

Choice of Protective Materials

The penetration criterion of Eqs. (15) and (16) contains only a single material parameter for a given configuration in which m_1 and m_2 are specified, namely $c_2(\xi/c_2)_a$. The higher the value of $c_2(\xi/c_2)_a$, the greater the penetration resistance of the material. Table 1 provides pertinent material properties for a range of materials, some of which may be suitable for protection against meteoroids. The upper portion concerns relatively ductile materials, whereas the lower portion concerns high-strength materials.

For applications where the rear sheet is not under initial stress, suitable materials are annealed stainless steels or other materials of high ductility. When the rear sheet is under an initial stress, as in the case of tankage, then a tradeoff must be made between the strength-to-weight ratio σ/ρ_2 and the penetration resistance $c_2(\xi/c_2)_a$, as illustrated in Fig. 8, where the effects of pressurization are also shown. They are considerable in the case of these rather brittle materials. It appears from the Fig. 8 that, for example, aged 6Al4V titanium and aged 13V11Cr3Al titanium are superior tankage materials.

The front sheet exists only to fragment the incoming particle and cause a spread in the resultant debris. It does possess some penetration resistance of its own, however, for particles below a certain threshold will not penetrate it. Generally, the threshold is higher for harder materials. Thus, a front sheet should ideally be composed of a relatively hard, or aged, material.

It should be noted that numerous other constraints will enter into the final choice of materials, for example, their cost, the availability of the required gauge, the resistance to corrosion due to the environment, and the electrolytic compatibility of the material with the surrounding structure.

Table 1 Properties of materials

Material	Condition	Elongation %	Young's Modulus psi × 10^6	Yield Stress at 0.2% Offset, ksi	Yield Stress ksi	Ultimate Stress ksi	Desity lbs/in^3	Strength-to-weight Ratio inches		Speed of Sound km/sec	Penetration Resistance km/sec	
		ϵ	E	σ_{yt}	σ	σ_u	ρ	$\frac{E}{\sigma_y}$	$\frac{\sigma_{yt}}{\rho}$	c	$\left(\frac{\xi}{c}\right)_a$	$c\left(\frac{\xi}{c}\right)_a$
2024 Al	T4	12	10.5	40	50	62	0.1	210		5.12	0.083	0.425
AZ31B Mg	0	12	6.5	18	23	32	0.064	282		5.04	0.075	0.378
Pure Ti	0	18	15.5	55	60	65	0.163	254		4.88	0.132	0.644
8A11Mo1V Ti	0	9	15.5	135	140	145	0.158	110		4.95	0.093	0.46
6A14V Ti	0	8	16.0	126	130	134	0.160	123		5.0	0.082	0.41
5A12.5Sn Ti	0	8	15.5	110	110	115	0.162	141		4.89	0.075	0.367
8 Mn Ti	0	8	15.5	110	115	120	0.171	132		4.76	0.079	0.376
13V11Cr3Al Ti	0	8	14.5	120	125	130	0.174	116		4.56	0.284	0.383
0.1% Carbon St.	Hot Rolled	40	29.0	...	42	...	0.286	690		5.04	0.295	1.49
301, 302, 304, SS	0	40	29.0	30	55	75	0.286	527		5.04	0.324	1.63
301 SS	1/4 Hard	25	27.0	75	105	125	0.286	257		4.86	0.218	1.06
301 SS	1/2 Hard	15	26.0	110	135	150	0.286	194		4.77	0.105	0.55
301 SS	3/4 Hard	10	26.0	135	160	175	0.286	163		4.77	0.08	0.382
Copper	Hot Rolled	45	13.0	8	18	30	0.32	720		3.19	0.33	1.08
Beryllium	Cross Rolled	5.5	44.0	...	70	...	0.067	630		12.8	0.03	0.384
2014 Al	T6	6	10.5	58	60	65	0.101	175	58	5.12	0.058	0.297
6061 Al	T6	8	9.9	35	40	42	0.098	247	36	4.95	0.059	0.292
7075 Al	T6	7	10.3	66	70	76	0.101	147	66	5.08	0.068	0.345
AZ31B Mg	H24	6	6.5	29	35	39	0.064	186	45	5.04	0.055	0.277
6A14V Ti	Aged	3	16.0	143	150	157	0.160	107	89.5	5.0	0.056	0.28
13V11Cr3Al Ti	Aged	4	14.5	170	180	190	0.174	80.5	97.5	4.56	0.065	0.297
6A16V2Sn Ti	Heat Treated	1.5	16	175	180	190	0.162	89	108	4.96	0.04	0.196
17-7PH SS	TH1050	3	29.0	150	165	180	0.276	176	54.3	5.12	0.062	0.215
301 SS	Hard	8	26.0	140	160	170	0.286	163	49	4.76	0.062	0.324
301 SS	Cryoformed	6	25.0	190	200	210	0.286	125	66.5	4.68	0.07	0.328
301 SS	Cryoformed and aged	1.5	25.0	260	260	260	0.286	96	91	4.68	0.043	0.201

The latter constraint makes it desirable to use front and rear sheets of the same metal.

Calculation of Protection Requirements

Having now obtained a penetration criterion for a double-walled structure, we are able to make estimates of the total protection required for a given vehicle and mission. By using the penetration criterion of Eqs. (15) and (16), it can be shown that the mass m_c that will just penetrate the double wall is

$$m_c = 1.44c_2(\xi/c_2)_a m_2 S^2/V_n; \quad m_1/\rho d > 1 \tag{19}$$

$$m_c = \left[\frac{1.44(\pi/6)^{1/3}c_2(\xi/c_2)_a m_1 m_2 S^2}{\rho^{2/3}V_n}\right]^{3/4}; \quad m_1/\rho d < 1 \tag{20}$$

Here, it has been assumed that the normal velocity component

$$V_n = V\cos\varphi \tag{21}$$

is responsible for penetration, where φ is the angle of incidence measured from the normal. This critical mass depends on the wall properties, as well as upon the angle of incidence φ, particle velocity V, and density ρ. The two latter quantities are distributed as shown in the histograms of Figs. 9a and 9b. At worst, the particles are normally incident, whereas at best, they may be considered to be isotropic so that their angle of incidence on a plane is distributed as $\sin\varphi$. To account for these distributions, the following Monte Carlo method has been used.

Basically, given the structural configuration, a number of particles are generated by a random number generator such

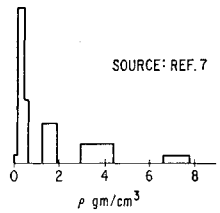

Fig. 9a Particle density distribution.

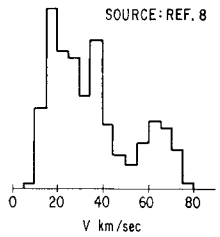

Fig. 9b Particle velocity distribution.

that their properties V, ρ, and φ obey the given distributions. Then, the probability of not encountering a particle of mass m_e or greater is given by the Poisson distribution

$$P_0 = \exp[-A\sum_i N_i T_i] \tag{22}$$

where A is the exposed area and T_i is the exposure time. The quantity N_i represents the meteoroid environment and is the number of particles of mass m_e or greater encountered per unit area per unit time. Usually N_i is expressed as

$$N_i = 10^{-a_i \pm \delta_i} m^{-b_i \pm \gamma} \tag{23}$$

where the subscript i is intended to account for various flux types (asteroidal or cometary) and flux durations, and δ_i and γ_i denote the possible errors in the flux. In this Monte Carlo procedure, δ_i and γ_i are assumed to be the standard deviations of a Gaussian flux distribution, and every particle is accorded a flux constant consistent with that distribution. For each structural configuration, the mean of all the computed probabilities will represent the probability of no penetrations occurring. If P_0 is nearly unity, then it can be shown that the probability P_1 of encountering one or fewer particles is approximately

$$P_1 \approx P_0(2 - P_0) \tag{24}$$

As an example of typical protection requirements, consider a Mars mission of 180 days duration where the exposed area of the sterilization canister forebody is 9 m². By using the flux given in Ref. 9, and the method described above, the results of Table 2 are obtained. They represent the minimum protection requirements necessary to achieve the indicated values of P_0 and P_1. The ranges in probability are due to the assumption of a unidirectional flux, on the one hand, and an isotropic flux, on the other hand. An estimate has also been made of the support structure weight required to maintain the spacing between the front and rear sheets. Other constraints such as minimum available gage, material compatibility, or pressurization may well dictate the use of different materials with a corresponding increase in weight. This example is intended solely to illustrate the type of results and weights to be expected.

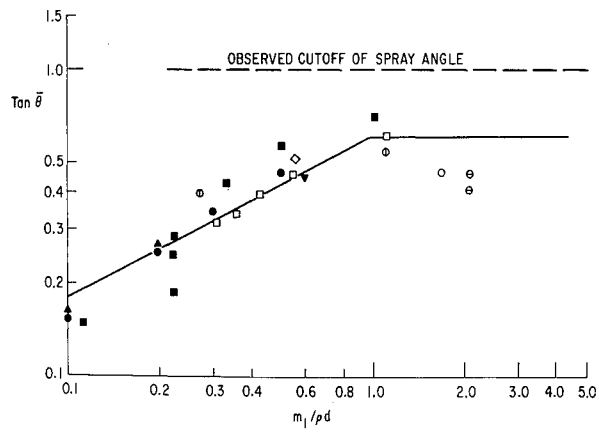

Fig. 10 Correlation of average cone angle of spray.

Table 2 Protection requirements for a sterilization canister forebody on a Mars mission

Spacing between front and rear sheets $\frac{1}{2}$ in.; support structure weight 5 lb
1) 0.002 in. 301 SS (annealed) rear sheet 0.002 in. 301 SS ($\frac{1}{4}$ hard) front sheet $0.996 < P_0 < 0.9985$, $0.999992 < P_1 < 0.999998$ $m_1 + m_2 = 16$ lb
2) 0.002 in. 301 SS ($\frac{1}{4}$ hard) rear sheet 0.002 in. 301 SS ($\frac{1}{4}$ hard) front sheet $0.994 < P_0 < 0.996$, $0.99998 < P_1 < 0.999993$ $m_1 + m_2 = 16$ lb
3) 0.005 in. Ti (commercially pure) rear sheet 0.005 in. 6Al4V Ti (aged) front sheet $0.9945 < P_0 < 0.9975$, $0.99999 < P_1 < 0.999996$ $m_1 + m_2 = 21.8$ lb

Appendix: Determination of the Average Cone Angle of the Spray

Results of various hypervelocity experiments[2,3] concerning the impact of particles into the targets indicate that the semivertex angle of the spray θ_m is rarely more than 45°. The theoretical studies of Refs. 2 and 4 also exhibit this effect. When the target is thin compared with the particle diameter, the spray angle can be considerably less than 45°. The

Table 3 Guide to Fig. 10

Symbol	Projectile	Velocity km/sec	Target	Ref.
■	Aluminum cylinder	7 – 50	Aluminum	2
●	Cadmium sphere	6	Cadmium	2
▼	Porous Al sphere 0.483 gm/cc	6	Aluminum	2
▲	Aluminum cylinders	20	Aluminum	10
○	Porous Al sphere 0.4 gm/cc	40	Aluminum	11
⊖	Hollow Al spheres	...	Aluminum	11
⊕	Aluminum Cylinders	7.6	Aluminum	12
◇	Iron cylinders	7.6	Iron	12
□	Aluminum cylinders	15	Multiple layers of Al, Be, Pb and Plexiglass	4

experimental results also indicate that the spray angle is not highly dependent on the impact velocity, as long as the velocity is high enough that the particle fragments. At lower velocities, the particle tends to emerge from the sheet in a relatively undamaged condition.

The average cone angle $\bar{\theta}$, defined in the sense of Eq. (2), is not derivable from the experimental results so far conducted. It can be estimated, however, from theoretical studies which have used hydrodynamic computer codes.[2,4,10-12] One of the results of these investigations is the distribution of momentum in the spray after impact. The average cone angle may be derived from the momentum distributions $D(r)$ in the form

$$\tan\bar{\theta} = \int_0^\infty r^2 D(r)dr \Big/ S \int_0^\infty rD(r)dr \qquad \text{(A1)}$$

where S is the distance from the front sheet at which $D(r)$ was originally computed. The results thus obtained were correlated with various nondimensional quantities. The most adequate correlation appears to be with the quantity $m_1/\rho d$. The correlation of $\tan\bar{\theta}$ with m_1 has previously been observed by Riney and Halda.[4] In addition, Madden[1] also found on theoretical grounds that $\tan\bar{\theta}$ was proportional to $m_1/\rho d$. The points derived from Eq. (A1) are shown in Fig. 10 and in Table 3. A satisfactory fit of the points yields the line

$$\tan\bar{\theta} = 0.6(m_1/\rho d)^{1/2} \qquad \text{(A2)}$$

Because the average cone angle must have a cutoff below $\bar{\theta} = 45°$, we have chosen, on the basis of the points so far obtained, to set the cutoff point at $m_1/\rho d = 1.0$. Thus, the average cone angle $\bar{\theta}$ is given by

$$\tan\bar{\theta} = \begin{cases} 0.6(m_1/\rho d)^{1/2}; & m_1/\rho d < 1 \\ 0.6 \quad\quad\quad\quad\; ; & m_1/\rho d > 1 \end{cases} \qquad \text{(A3)}$$

References

[1] Madden, R., "Ballistic Limit of Double-Walled Meteoroid Bumper Systems," TN D-3916, April 1967, NASA.

[2] McMillan, A. R., "Experimental Investigations of Simulated Meteoroid Damage to Various Spacecraft Structures," TR 66-67, NASA CR-915, Nov. 1966, General Motors Defense Research Lab., Santa Barbara, Calif.

[3] Lundeberg, J. F., Stern, P. H., and Bristow, R. J., "Meteoroid Protection for Spacecraft Structures," D2-24056, NASA CR-54201, Oct. 1965, Boeing Co., Seattle, Wash.

[4] Riney, T. D. and Halda, E. J., "Effectiveness of Meteoroid Bumpers Composed of Two Layers of Distinct Materials," *AIAA Journal*, Vol. 6, No. 2, Feb. 1968, pp. 338–344.

[5] Witmer, E. A. et al., "Large Dynamic Deformations of Beams, Rings, Plates, and Shells," *AIAA Journal*, Vol. 1, No. 8, Aug. 1963, pp. 1848–1857.

[6] Balmer, H. A., "Improved Computer Program—Depross 1, 2, and 3—to Calculate the Dynamic Elastic-Plastic Two-Dimensional Responses of Impulsively-Loaded Beams, Rings, Plates, and Shells of Revolution," ASRL TR 128-3, Aug. 1965, Massachusetts Institute of Technology, Aeroelastic and Structures Research Lab., Cambridge, Mass.

[7] Volkoff, J. J., "Protection Requirements for the Resistance of Meteoroid Penetration Damage of Interplanetary Spacecraft Systems," TR 32-410, July 1964, Jet Propulsion Lab., Pasadena, Calif.

[8] Deyarmond, A. B. and Ingram, G. E., "A New Approach to Estimating the Effect of the Meteoroid Hazard on Spacecraft Reliability," paper EN-4, *Proceedings of the National Symposium of the American Astronautical Society*, Vol. I, Huntsville, Ala., June 1967.

[9] Weider, D. K. and Hasseltine, C. L., "Natural Environment Design Criterion Guidelines for MSFC Voyager Spacecraft for Mars 1973 Mission," TMX-53616, 1967, NASA.

[10] Bjork, R. L., "Review of Physical Processes in Hypervelocity Impact," *Proceedings of the 6th Hypervelocity Impact Symposium*, Vol. 2, Pt. 1, Aug. 1963, pp. 1–58; in particular, p. 40.

[11] Woodall, S. R., "A Numerical Method for Analyzing Meteoroid Two-Sheet Structural Configuration Impact Problems," Mechanics Section TM 067-6A, Aug. 1967, General Electric Co., Space Sciences Lab., King of Prussia, Pa.

[12] Riney, T. D. and Heyda, J. F., "Theoretical Calculations for Meteor Bumper Systems," *Proceedings of the AIAA Symposium on Structural Dynamics and Aeroelasticity*, AIAA, New York, 1965, pp. 406–418.